Sound Radiation from Circular Stretched Membranes in Free Space*

J. H. STRENG

Philips Research Laboratories, 5600 JA Eindhoven, The Netherlands

Some radiation characteristics of circular stretched vibrating membranes are calculated. The calculations include the fluid loading effects of air, which are of essential influence on the membrane's vibrational behavior in the frequency range around $ka = 1$. Results are presented to show that the sound radiation of the most prominent representative of stretched-membrane loudspeakers, namely, the electrostatic push–pull loudspeaker, may be predicted very accurately. The full numerical procedure is supplied in the Appendix.

LIST OF SYMBOLS

a	=	membrane radius
c_0	=	sound velocity in air
c_a	=	compliance
d_0	=	membrane–electrode distance in electrostatic loudspeaker
$D(\theta)$	=	directivity function
DI	=	directivity index
f	=	frequency
$F(r)$	=	axial driving force per unit area
k	=	wave number in air; $= 2\pi f/c_0$
$p(r, z)$	=	sound pressure in point (r, z)
$p_+(r), p_-(r)$	=	surface sound pressure at $z \downarrow 0$, $z \uparrow 0$
s	=	segment of circle; $0 < s \leqslant a$
T	=	membrane tension
$v(r, z)$	=	particle velocity at (r, z)
z_a, z_s	=	specific acoustic impedance
α	=	normalized wave number in stretched membrane
β	=	normalized wave number in air; $= ka$
γ	=	fluid loading parameter
$\eta(r)$	=	membrane deflection
θ	=	off-axis angle
λ	=	wavelength in air
ρ_0	=	density of air
ρ_m	=	membrane surface density
τ_n	=	series expansion coefficient
ω	=	circular frequency

* Presented at the 84th Convention of the Audio Engineering Society, Paris, France, 1988 March 1–4.

0 INTRODUCTION

Stretched-membrane loudspeakers are known for their superior quality in sound reproduction systems. The electrostatic push–pull loudspeaker in particular, which is basically a stretched-membrane doublet radiator, ranks among the best transducers in the audio field. Because of this superiority, it is of interest to have a fundamental analysis of the sound radiation from stretched membranes, and especially of the unbaffled (doublet) version. (For reasons of geometric simplicity we only consider a circular shape and axisymmetric variations.) As a first approach one might consider the vibrating membrane as a circular disk, vibrating in free air. The fundamental analysis of such a transducer was given some 46 years ago by Bouwkamp [1], and his analysis was used by several authors (see, for example, [2]–[4]) to study or file the sound radiation properties of a circular vibrating disk. Although this approach may give some qualitative insight (see, for example, the analysis by Walker [5]), we will see in this paper that the rigid-piston model, when applied to the stretched-membrane problem, is basically incorrect (quite apart from the difficulty of calculating the radiated sound field from an unbaffled piston). As was pointed out in a recent paper [6], this discrepancy is mostly due to the following differences between piston and membrane.

1) Unlike the piston, the stretched membrane has no bending stiffness. This implies that the membrane's reaction to the air load has an essentially local character. In contrast, the piston will show a global reaction to the (integrated) surface sound pressure. We will see that these differences are most pronounced in the low-

and midfrequency range, where the vibrational behavior of the stretched membrane is strongly influenced by the surface sound pressure.

2) Another important difference results from the edge behavior of the transducer. Bouwkamp [1] showed that the radial velocity of the air particles on the piston surface will become singular at the piston edge. This effect will cause air turbulence and physical nonlinearities, which is intuitively understood. In contrast, it was shown in [6] that the stretched edge-clamped membrane produces zero particle velocity at the edge. Roughly speaking, the vibrating piston is likely to produce a "hissing" sound at the edge, whereas the stretched membrane produces "only silence" at the edge.

Due to these differences it will be clear that the analysis of the vibrational behavior of the stretched membrane calls for a nonpistonlike approach. Even more, due to the strong interaction of membrane and air it is necessary to solve the complete coupled system of membrane vibrations, air load, and sound propagation all at once. Although this problem has received attention in the literature (see, for example, [7]), the analysis is usually focused on extreme situations, such as very high or very low frequencies. In our case, however, we deal with strong interactions in the middle frequency range (membrane diameter comparable to in-air wavelength). Thus the extreme-situation attack of the problem is not satisfactory, and the full fundamental theory must be applied. In a recent paper [6] this theory has been worked out and molded for numerical implementation. We will see that the fundamental approach gives very good results for the prediction of sound radiation of circular stretched membranes in the range of $0 < ka < 5$, and this makes a numerical algorithm based on this theory attractive for computer-aided design. For the high-frequency range, say $ka \geq 5$, one should use the familiar high-frequency approximation, that is, the air load is determined by the plane-wave impedance $\rho_0 c_0$ (see [6]). This is a well-known technique that will not be covered in this paper.

In Sec. 1 we examine the basic configuration and governing equations, as well as a description of the method for calculating the solution of the coupled system. (The numerical procedure is given in the Appendix; the mathematical background is given in [6].) In Sec. 2 we derive expressions for the near-field and far-field characteristics which, in turn, will be used in Sec. 3, where we examine some results. An important aspect of full-range (electrostatic) membrane loudspeakers, that is, the prevention of sound-focusing effects in the higher frequency range by means of partial drive of the membrane, is also covered in Sec. 3.

1 THE VIBRATING STRETCHED MEMBRANE IN AIR

1.1 Description of Membrane Vibration and Air-Loading Effects

The equation of motion of the vibrating edge-clamped membrane follows directly from a balance of forces acting upon the membrane (Fig. 1). If the membrane excursion along the radius $0 \leq r \leq a$ is denoted by $\eta(r)$, then $\eta(r)$ is the solution of the following differential equation (assuming a harmonic time dependence $e^{j\omega t}$) [6]:

$$T\nabla_2^2\eta(r) + \omega^2\rho_m\eta(r) - j\omega z_s\eta(r) + F(r) - (p_+(r) - p_-(r)) = 0, \quad r \leq a, \quad \eta(a) = 0 \tag{1}$$

where the various parameters are defined as follows. The first term in Eq. (1),

$$T\nabla_2^2\eta(r) = T\left[\frac{\partial^2}{\partial r^2}\eta(r) + \frac{\partial}{r\,\partial r}\eta(r)\right] \tag{2}$$

is the membrane-restoring force which drives the membrane back to its equilibrium position. This force is determined by the membrane tension T [N/m] and the membrane curvature $\nabla_2^2\eta(r)$. The second term in Eq. (1) denotes the membrane's inertial force, determined by the membrane density ρ_m [kg/m^2] and membrane acceleration. The third term accounts for effects, such as an additional viscous damping, which may be described by means of a specific acoustic impedance z_s [N · s/m^3]. The fourth term, $F(r)$ [N/m^2], denotes the external driving force in the positive z direction per unit area. In this paper we only consider the following two forms for the driving force:

$$F_1(r) = F, \qquad 0 \leq r \leq a$$
$$F_2(r) = \begin{cases} F, & 0 \leq r/a \leq s \\ 0, & s \leq r/a \leq 1 \end{cases} \tag{3}$$

which means that we will either drive the entire membrane [$F_1(r)$] or a circular inner section of the membrane [$F_2(r)$]. The driving force will be of constant amplitude F along the driven section. The last term on the left-hand side of Eq. (1) denotes the pressure difference across the membrane; $p_+(r)$ denotes the surface sound

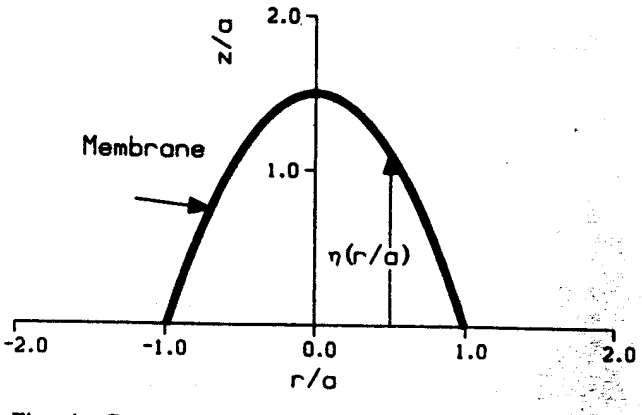

Fig. 1. Geometry of circular stretched membrane. The stretched membrane M (tension T, surface density ρ_m) is clamped at its circumference $r = a$. The membrane deflection in the z direction is denoted by $\eta(r)$.

pressure at $z = 0$, whereas $p_-(r) = -p_+(r)$ is the surface sound pressure at $z = 0$. As stated in the Introduction, this surface pressure term must be handled with great care in the analysis of vibrating stretched membranes because the interaction between the membrane and the surrounding air is very important.

The sound pressure $p(r, z)$ at a point (r, z) in the surrounding air must of course satisfy the Helmholtz equation:

$$\nabla_3^2 p(r, z) + k^2 p(r, z) = 0$$

$$p(r, 0^+) = p_+(r), \qquad r \leq a \tag{4}$$

$$p(r, 0^-) = p_-(r), \qquad r \leq a$$

where

$$\nabla_3^2 p(r, z) = \frac{\partial^2}{\partial r^2} p(r, z) + \frac{\partial}{r\,\partial r} p(r, z) + \frac{\partial^2}{\partial z^2} p(r, z). \tag{5}$$

Finally, we have the well-known coupling constraint

$$\left.\frac{\partial p(r, z)}{\partial z}\right|_{z=0^+} = \left.\frac{\partial p(r, z)}{\partial z}\right|_{z=0^-} = \omega^2 \rho_0 \eta(r), \qquad r \leq a \tag{6}$$

which states that the normal component of the air particle velocity equals the membrane velocity at the membrane–air interface (ρ_0 [kg/m^3] is the density of air). The problem now is to solve Eqs. (1), (4), and (6) simultaneously. We see that in these three equations the surface pressure $p_+(r) = -p_-(r)$ plays an essential role. Therefore, in order to find a solution, we have to focus on a solution for the surface pressure.

1.2 Calculation of Surface Pressure

The line of work for the construction of a solution is as follows. First we express the membrane excursion $\eta(r)$ in terms of the surface pressure $p_+(r)$ by means of a suitable Green function $G_1(r|r_0)$. This results in the expression

$$\eta(r) = \int_0^a p_+(r_0) G_1(r|r_0) r_0 \, dr_0 \tag{7}$$

which is a formal solution of Eq. (1). (Details of the function $G_1(r|r_0)$ may be found in [6].) Next we express the sound pressure $p(r, z)$ as a formal solution of Eq. (4), in terms of $p_+(r)$, by means of the free-field Green function $G_2(r, z|r_0, z_0)$, which yields

$$p(r, z) = \int_0^a p_+(r_0) \left[\frac{\partial}{\partial z_0} G_2(r, z|r_0, z_0)\right]\Big|_{z_0=0} r_0 \, dr_0 . \tag{8}$$

(Again, details of $G_2(r, z|r_0, z_0)$ will be found in [6].) By applying Eq. (6) to Eq. (8) we obtain a second expression for $\eta(r)$,

$$\eta(r) = \frac{1}{\omega^2 \rho_0} \int_0^a p_+(r_0) \left\{\frac{\partial}{\partial z}\left[\frac{\partial}{\partial z_0} G_2(r, z|r_0, z_0)\right]_{z_0=0}\right\}_{z=0^-,0^+} r_0 \, dr_0 . \tag{9}$$

Now, equating Eqs. (7) and (9) we obtain an integral equation for $p_+(r)$. In [6] it is shown that this equation can be solved accurately be means of a power series expansion for $p_+(r)$,

$$p_+(r) = \frac{a\omega^2 \rho_0 F}{T} \sum_{n=1}^{N} \frac{\tau_n (a^2 - r^2)^{n+1/2}}{2^{n+1/2}\Gamma(n + 3/2)}, \qquad N \to \infty \tag{10}$$

where $\Gamma(x)$ is the gamma function of argument x. The introduction of Eq. (10) enables us to transform the integral equation into an infinite set of linear equations from which any number of coefficients τ_n may be determined by means of a truncation at finite N and a least-squares procedure. The numerical procedure for this is given in the Appendix.

2 SOUND-FIELD CHARACTERISTICS

2.1 Sound Pressure Level (SPL) and Directivity

The SPL (expressed in dB re 2×10^{-5} N/m^2) is calculated straightforwardly from the sound pressure $p(r, z)$ which, in turn, is given in Eq. (29) and reads

$$p(r, z) = \frac{a^3 \omega^2 \rho_0 F}{T} \sum_{n=1}^{N} \tau_n \times \int_0^{\infty} \left(\frac{1}{\mu}\right)^{n+1/2} J_0\left(\frac{\mu r}{a}\right) J_{n+1/2}(\mu) e^{-j\sigma z/a} \, d\theta$$

$$\sigma = \begin{cases} \sqrt{\beta^2 - \mu^2}, & \mu \leq \beta \\ -j\sqrt{\mu^2 - \beta^2}, & \mu > \beta \end{cases} \tag{11}$$

where $J_0(x)$ and $J_{n+1/2}(x)$ denote Bessel functions of the first kind and of order 0 and $n + 1/2$, respectively. The angular distribution (or directivity function) is usually determined in the far field. This means that we have to calculate $p(r, z)$ for large values of $R = \sqrt{r^2 + z^2}$. Although it is possible to use Eq. (11) for the calculation of $p(r, z)$ in the far field, it is common practice to introduce an asymptotic approximation in order to simplify the calculations. The main reason for doing this is easily understood: we do know that the far-field waves have a spherically diverging character,

thus they must contain a term e^{-jkR}/R. This term is normally left out in the definition of the directivity function (see [4]), because it supplies no essential information. The directivity function then only contains angular information, so in our case (axisymmetric) the only spatial coordinate in the directivity function is the off-axis angle θ. Without going into detail on the mathematics, it must be mentioned that the following asymptotic far-field expression can be derived.

$$p(r, z) = \frac{e^{-jkR}}{R} D(\theta) , \qquad r = R \sin\theta , \quad z = R \cos\theta \tag{12}$$

where the directivity function $D(\theta)$ is defined as

$$D(\theta) = j \frac{a^4 \omega^2 \rho_0 F}{T} ka \cos\theta \times \sum_{n=1}^{N} \tau_n \left(\frac{1}{ka \sin\theta} \right)^{n+1/2} J_{n-1/2}(ka \sin\theta) . \tag{13}$$

For $\theta = 0$ the limiting form of Eq. (13) is found to be

$$D(0) = \lim_{\theta \to 0} D(\theta) = j \frac{a^4 \omega^2 \rho_0 F}{T} ka \times \sum_{n=1}^{N} \frac{\tau_n}{2^{n+1/2} \Gamma(n + 1/2)(2n + 3)} . \tag{14}$$

The on-axis directivity index DI is, as usual, calculated from the ratio of (far-field) on-axis intensity and average (far-field) intensity, which is easily calculated to be

$$DI = 10 \log_{10} \frac{|D(0)|^2}{\int_0^{\pi/2} \sin\theta |D(\theta)|^2 \, d\theta} \quad [dB] . \tag{15}$$

2.2 Radiation Impedance

The radiation impedance is usually calculated from the ratio of surface pressure and surface velocity, integrated over the radiating area. In the case of stretched-membrane radiation, however, this definition will cause problems because the membrane deflection is likely to show nodal lines, which will cause a singularity in the specific acoustic impedance. (In the next section we see that this effect truly occurs.) Let us therefore examine the "averaged" specific acoustic impedance z_a which is calculated from the ratio of averaged surface pressure $\langle p_+(r) \rangle$ and averaged membrane velocity $j\omega \langle \eta(r) \rangle$:

$$z_a = \frac{\langle p_+(r) \rangle}{j\omega \langle \eta(r) \rangle} = \frac{\int_0^a p_+(r) r \, dr}{j\omega \int_0^a \eta(r) r \, dr} . \tag{16}$$

Since in the case of rigid piston vibration the averaged specific acoustic impedance according to Eq. (16) is known (see, for example, [4]), we may compare the piston impedance and the membrane impedance directly from this equation (which is done in Sec. 3.2).

3 RESULTS

3.1 On-Axis SPL and Influence of Parameters

In this section we focus on the most widely used loudspeaker characteristic, its free-field sound pressure level (SPL) at 1 m on axis. In Fig. 2 we see the calculated response of a theoretical stretched-membrane loudspeaker with parameters $T = 100$ N/m, $\rho_m = 0.02$ kg/m^2, $a = 0.125$ m, $z_s = 0$ N · s/m^3, and a driving force $F = 1$ N/m^2. Calculations are carried out up to $ka = 5$. The frequency plot in Fig. 2 shows a typical stretched-membrane response. At the low-frequency side, say $f < 50$ Hz or $ka < 0.1$, we have an 18-dB/octave increase. The membrane's vibrational behavior is mass-controlled in this region, which resembles the free-piston behavior [2]–[4], where the mass component of the radiation impedance is constant in the low-frequency region and the resistive component shows a ω^4 dependence. At a frequency $f \approx 75$ Hz we see a sharp resonance peak, mainly determined by the membrane tension T and the mass of the air load. (The influence of the membrane density ρ_m is negligible in this region.)

Next we take a look at the high-frequency end, say, $f > 1$ kHz or $ka > 2$, where we see a smooth 6-dB/octave increase. In this region one can apply plane-wave theory [6], that is, the air load becomes purely resistive with a specific acoustic resistance $\rho_0 c_0$, and the radiated power is more and more focused on axis. Neither the very low nor the very high frequency range

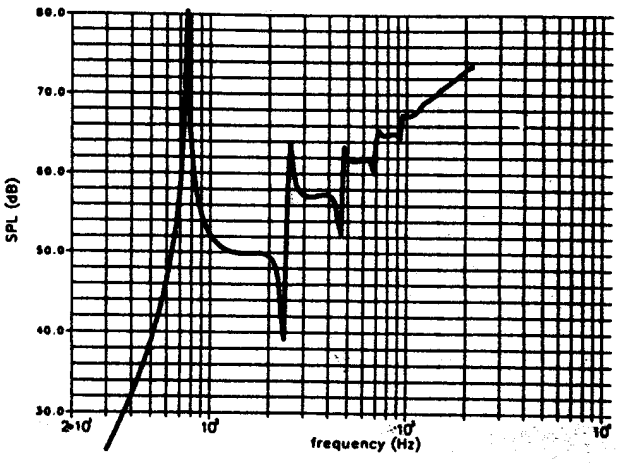

Fig. 2. On-axis SPL of stretched-membrane loudspeaker. Response at 1 m on axis with parameters $T = 100$ N/m, $\rho_m = 0.02$ kg/m^2, $a = 0.125$ m, $z_s = 0$ N · s/m^3, and $F = 1$ N/m^2. Calculations were carried out up to $ka = 5$.

is of essential importance for our loudspeaker (insufficient sound radiation at the lower frequencies, undesired focusing effect at high frequencies). Instead, we have to examine the situation in the region between the basic resonance and, say, $ka = 2$ (that is, between 70 Hz and 1 kHz approximately), where we see a number of membrane resonance effects. It may be interesting to see what happens at the membrane surface in the frequency range closely around one of these resonances. Let us therefore examine the situation of Fig. 2 at the following frequencies: $f = 210$, 245, 255, and 300 Hz. In Fig. 3 the calculated surface pressure and membrane deflection are shown for these frequencies. At 210 Hz [Fig. 3(a)] we see that the surface pressure and the membrane deflection show a nodal line in their amplitude, and that they are either in phase or in opposite phase with the driving force, indicating that the vibration is almost purely mass-controlled. As frequency increases to 245 Hz [Fig. 3(b)], the nodal lines move inward radially: the nodal pressure line moves inward more "rapidly" than the nodal deflection line and eventually "passes" the nodal deflection line. The whole system behaves like two (balance-) coupled mass-spring systems. So if frequency increases, we see that a typical coupled mass-spring characteristic appears: an antiresonance frequency with the corresponding dip in the SPL characteristic, followed by a sharp resonance frequency. At 255 Hz [Fig. 3(c)] we have passed the resonance frequency, which is shown by the 180° phase jump in both pressure and deflection. It appears that

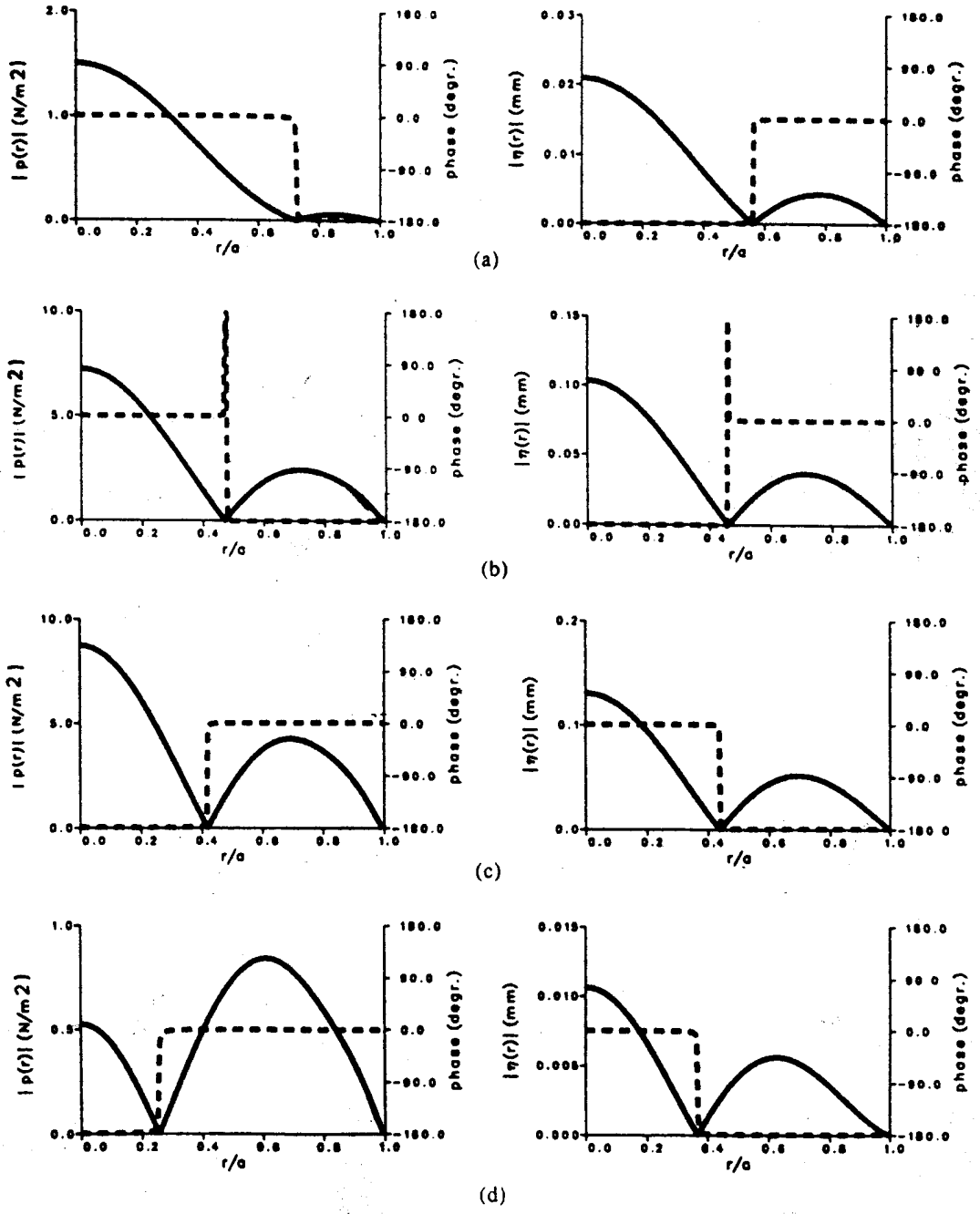

Fig. 3. Calculated surface pressure and membrane deflection. Solid lines—modulus; dashed lines—phase. (a) 210 Hz. (b) 245 Hz. (c) 255 Hz. (d) 300 Hz. Membrane parameters as in Fig. 2.

resonance effects occur very close to the point where the nodal pressure line "passes" the nodal deflection line. At 300 Hz (Fig. 3(d)] we have a situation that is more or less symmetric with the one at 210 Hz and as frequency increases, a second nodal deflection line will show up "followed" by a nodal pressure line, which will eventually "cause" the next resonance, and so on. Of course, the nodal lines become less pronounced at higher frequencies due to the fact that the air load becomes more and more resistive, which eventually heavily damps the vibration.

Another point of interest is the influence of parameters. Of course, the effects may be studied qualitatively from a simpler model, but the exact quantitative effects can only be determined from the coupled model. Let us first vary the membrane tension T. Fig. 4 shows the effect of a variation of tension by 50%, starting at $T = 100$ N/m. Comparing the curves in Figs. 4 and 2, we see that the most important effect due to tension variation is a shift of the total SPL curve along the 6-dB/octave line, so the membrane tension merely affects the position of resonance frequencies and does not affect the average SPL.

Next we vary the membrane density, that is, we increase the density by a factor of 10 (Fig. 5). The influence of an increasing density is first noticed at the high-frequency side, where the air load mass is negligible and the inertance effect (that is, a $1/\omega^2$ or -12-dB/octave dependence) causes a high-frequency rolloff of -6 dB/octave. The low-frequency side is not affected until the membrane weight becomes of the same order of magnitude as the air load mass, which is some 0.125 kg m^{-2} in our case. In Fig. 5 it is clear that the increased membrane weight introduces the expected high-frequency rolloff and lower resonance frequencies.

Finally we look at the influence of z_s. For that purpose we examine the case where z_s is purely resistive (which is the case when we use additional acoustic damping), and after that we introduce a negative compliance, which occurs in a voltage-driven electrostatic loudspeaker [8]. In Fig. 6 we see the influence of damping. We see that the sharp resonances diminish as damping increases, and a damping of some 40 rayl is needed to realize a critical damping of the lowest resonance. As an aside it must be mentioned that since the analysis is exact in this case, it may be possible to reverse the procedure, that is, to estimate acoustic impedances z_s by means of "tuning" the calculated response to the measured response.

The influence of a negative compliance c_a, which introduces an impedance $z_s = -1/j\omega c_a$, is of course most pronounced in the region where $1/c_a > \omega^2\rho_m$, as is easily seen after substitution of z_s into Eq. (1). There is an upper bound on the value of $1/c_a$, which follows from Eq. (1) after substitution of $\omega = 0$ and $F(r) = 0$ [and consequently $p_+(r) = p_-(r) = 0$], which yields

$$T\nabla_2^2\eta(r) + \frac{1}{c_a}\eta(r) + \frac{1}{c_a}\eta(r) = 0, \qquad r \leq a,$$
$$\eta(a) = 0 \quad (17)$$

The solution of Eq. (17) is

$$\eta(r) = \begin{cases} 0, & a/\sqrt{Tc_a} \neq j_{0n} \\ CJ_0(j_{0n}r/a), & a/\sqrt{Tc_a} = j_{0n} \end{cases} \quad (18)$$

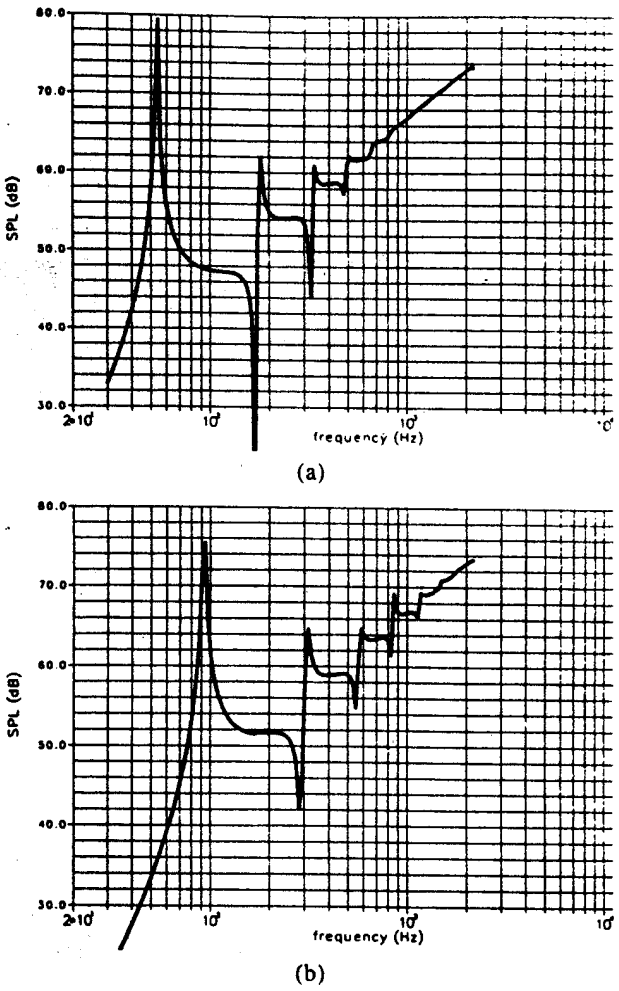

Fig. 4. Influence of tension variation on on-axis SPL. The on-axis response at 1 m is calculated for (a) $T = 50$ N/m; (b) $T = 150$ N/m.

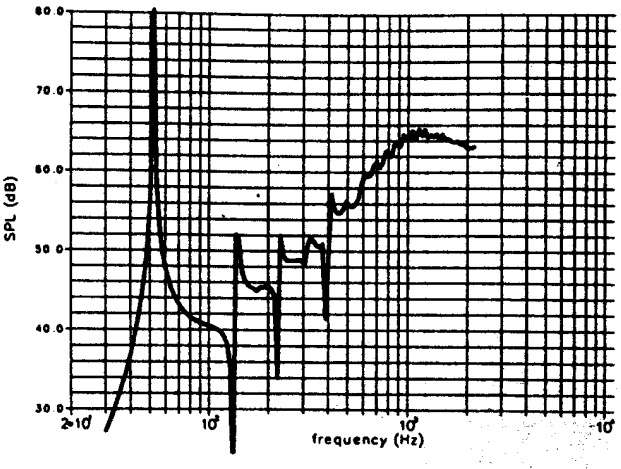

Fig. 5. Influence of membrane density variation on on-axis SPL. The on-axis response at 1 m is calculated for $\rho_m = 0.2$ kg/m^2.

where j_{0n} is the nth zero of the Bessel function J_0, and C is an arbitrary constant. From the solution we see that increasing the value of $1/c_a$ will yield an instability at zero frequency when $1/c_a = T/a^2 = 5.783T/a^2$. So for stable operation we have to satisfy $1/c_a < 5.783T/a^2$. If we combine this restriction with the previously found restriction on $1/c_a$ for the region of influence, then we see that we have to choose

$$\omega^2 \rho_m < \frac{1}{c_a} < \frac{5.783T}{a^2} \quad (19)$$

Substitution of the parameters from Fig. 2 yields that the region of influence is restricted to $f < 216$ Hz and the restriction for stable operation is $1/c_a < 37\,012$ N/m^3. In Fig. 7 we see the result obtained with the parameters from Fig. 2 plus an additional negative compliance. It will be clear that the negative compliance merely affects the basic resonance, and thus variation of the negative compliance is an elegant method to "tune" the resonance frequency without disturbing the rest of the on-axis SPL characteristic.

3.2 Radiation Impedance

In Sec. 3.1 we have seen that for very high and very low frequencies the membrane air load resembles the free-piston air load. For the frequency range in between, however, there is an essential difference. In Fig. 8 we see the averaged specific acoustic impedance (or normalized mechanical impedance) of the freely vibrating piston in air [4]. Here the transition from low frequencies ($ka < 0.1$) to higher frequencies ($ka > 2.0$) is very smooth. If we were to use the impedance characteristic of Fig. 8 as an approximation for the membrane air load, we would force the system to satisfy a prescribed interaction of membrane and air. Without going into detail on the mathematics, it must be mentioned that a uniform air load according to the free-piston impedance forces the membrane resonances (not the basic resonance) to increase by about an octave from the "real" value. The reason for this effect is of course the fact that if different parts of the membrane vibrate in opposite phase, then there will be a considerable amount of air that is "pumped" from one part to another and vice versa, without effectively contributing to the sound radiation. This air volume is thus responsible for a mass load with a rather local character, which is difficult to express in terms of a uniform load, especially close to the resonance frequencies where the average volume displacement may be very small, whereas there may still be a considerable local displacement. In Fig. 9 we see the "averaged" membrane-specific acoustic

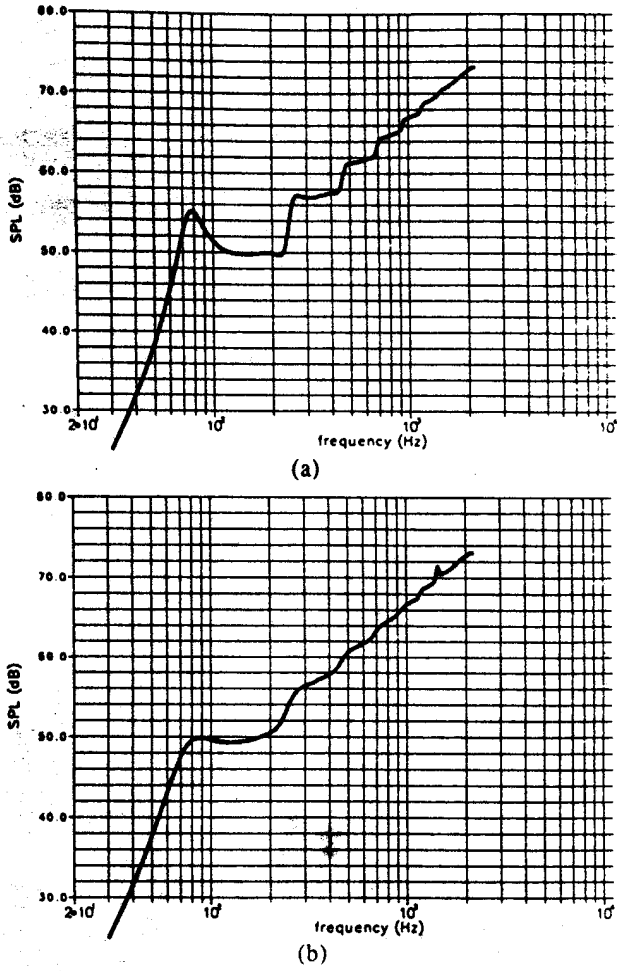

Fig. 6. Influence of damping on on-axis SPL. The on-axis response at 1 m is calculated for (a) $z_s = 20$ N · s/m^3; (b) $z_s = 40$ N · s/m^3.

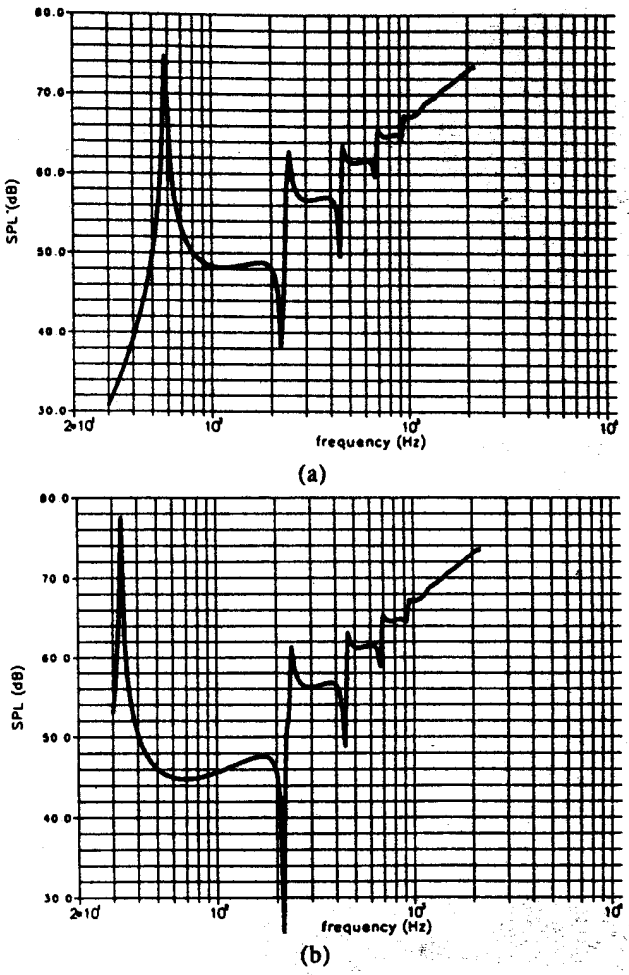

Fig. 7. Influence of negative compliance on on-axis SPL. The on-axis response at 1 m is calculated for (a) $1/c_a = 15\,000$ N/m^3; (b) $1/c_a = 30\,000$ N/m^3.

impedance (with parameters according to Fig. 2), calculated from Eq. (16). The extra mass load can be seen from the sharp peaks in the calculated impedance. The peaks are located near the membrane resonance frequencies, so if this result is compared with the data from Fig. 8, then it is easily understood that the mass component in these peaks will cause lower resonance frequencies. Since the positions of the resonance frequencies are strongly affected by the various parameters, it is impossible to determine an all-purpose membrane radiation impedance in the region around $ka = 1$.

3.3 Directivity Index and Polar Patterns

The directivity index and polar patterns are calculated straightforwardly from Eqs. (13)–(15). In Fig. 10 we see the polar patterns at $ka = 0.1$, 1, 3, and 5 with parameters according to Fig. 2. At low frequencies we have the usual doublet pattern [Fig. 10(a)] with a directivity index of 4.8 dB, whereas at higher frequencies the radiation becomes more and more directive. If we compare the results of Fig. 10 with the data of the freely vibrating piston [4], it turns out that membrane radiation is more directive than free-piston radiation. (Although very much alike, the directivity index for this membrane is about 1 dB larger at $ka = 5$.)

3.4 Some Aspects of the Design of a Circular Wide-Range Loudspeaker

In this section we examine some design aspects of a (theoretical) wide-range membrane loudspeaker, based on the parameters we have used previously (Fig. 2). We assume that the membrane diameter, tension, and weight are already chosen such that the desired basic resonance frequency and high-frequency rolloff are obtained. We will assume a uniform driving force $F = 1$ N m^{-2}, so the basic on-axis SPL characteristic is given in Fig. 2. First of all we have to supply appropriate damping to tackle the resonance effects. From Fig. 6 we see that we should use a damping of some 40 rayl. The next problem we encounter is the focusing effect at higher frequencies (see Sec. 3.3). Fig. 11 shows the calculated SPL at 1 m and 45° off axis. We see that the comb effect is already very pronounced at 2 kHz, so additional measures have to be taken. We will follow the "traditional" approach, which is that we will use a partial drive of the membrane at higher frequencies in order to reduce the radiating area and, in consequence, to reduce the focusing effect. To this end we introduce a parameter s [see Eq. (3)], which defines the circular area $0 \leq r/a \leq s$ where the driving force is active. The calculated on-axis SPL at 1 m is given in Fig. 12(a), and the 45° off-axis SPL at 1 m in Fig. 12(b) for various

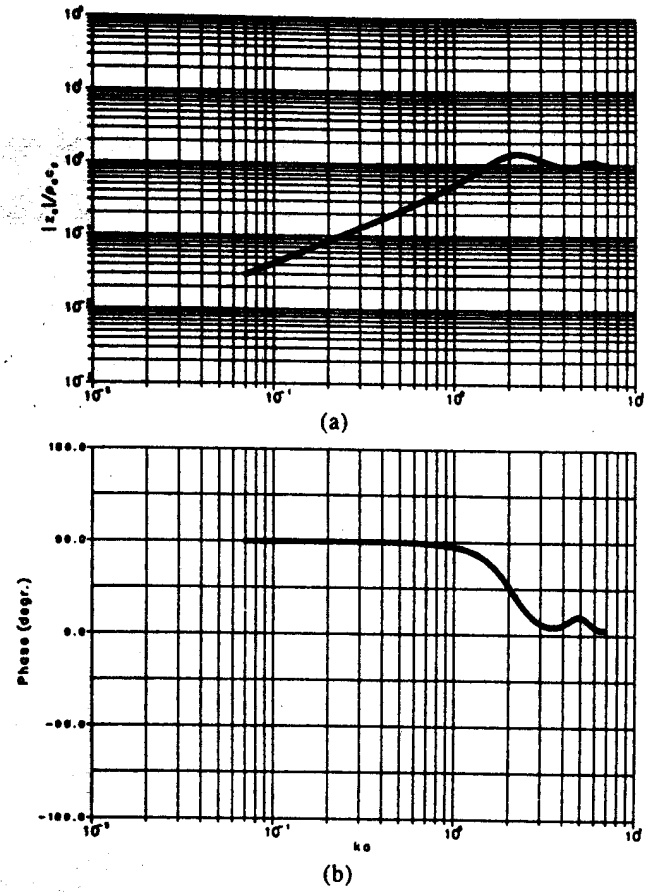

Fig. 8. Free-piston (normalized) specific acoustic impedance. (a) Modulus. (b) Phase.

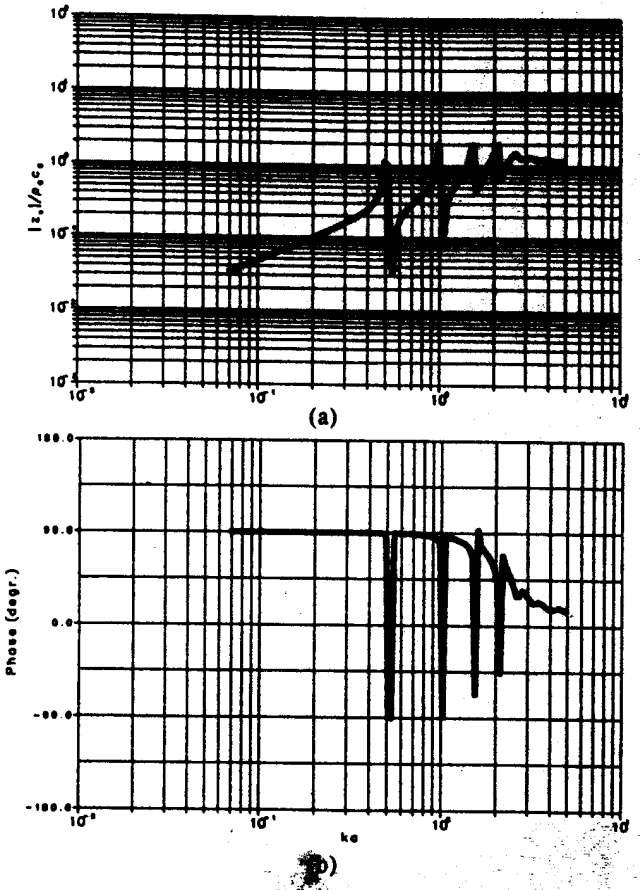

Fig. 9. Calculated (normalized) specific acoustic impedance of vibrating membrane. The radiation impedance is calculated for a membrane with parameters according to Fig. 2. (a) Modulus. (b) Phase.

values of s. The effect is, as expected, that a decrease of s gives a decreased SPL and a reduced focusing effect [indicated by a shift of the "comb dip" toward higher frequencies in Fig. 12.5]. We now see that a flat on-axis response may be approximated by "switching" to smaller radiating areas at higher frequencies, and that the focusing effect will automatically decrease. The complete design will of course consist of as many "segments" as possible to produce an optimal response. It must be emphasized that the response of the loudspeaker is less "smooth" as s decreases (see Fig. 12). This will strongly influence the choice of the switching frequencies, and since knowledge of the exact SPLs is important in this case, it will be clear that the exact theoretical analysis is very useful.

3.5 Electrostatic Push–Pull Loudspeakers

Up to this point we have only considered theoretical transducers, so we will be interested in the results for a "real" case. Therefore we examine a circular electrostatic push–pull loudspeaker with a membrane diameter of 250 mm (Fig. 13). The construction of the loudspeaker is quite traditional (see [8]): the thin stretched membrane M (measured tension $T = 73$ N/m, surface density $\rho_m = 0.02$ kg/m^2) is clamped between two stationary perforated electrodes E at a distance $d_0 = 2.3$ mm and charged by a dc source $V_0 = 1500$ V. The ac audio signal sources $V_1 = 300\sqrt{2}$ V drive the electrodes in opposite phase. The electrostatic driving force F_e on the membrane may be calculated from [8]

$$F_e = 2\varepsilon \frac{V_0 V_1}{d_0^2} = 2.13 \text{ N/m}^2 \qquad (20)$$

($\varepsilon \simeq 8.85 \times 10^{-12}$ is the dielectric constant of air). The negative compliance that occurs in this setup may be calculated from [8]

$$\frac{1}{c_a} = 2\varepsilon \frac{V_0^2}{d_0^3} = 3275 \text{ N/m}^3 . \qquad (21)$$

The impedance of the perforated electrodes depends on the geometry of the holes and on frequency. Formulas for the calculation of screen impedances may be found in [4]. Finally we have to take into account the influence

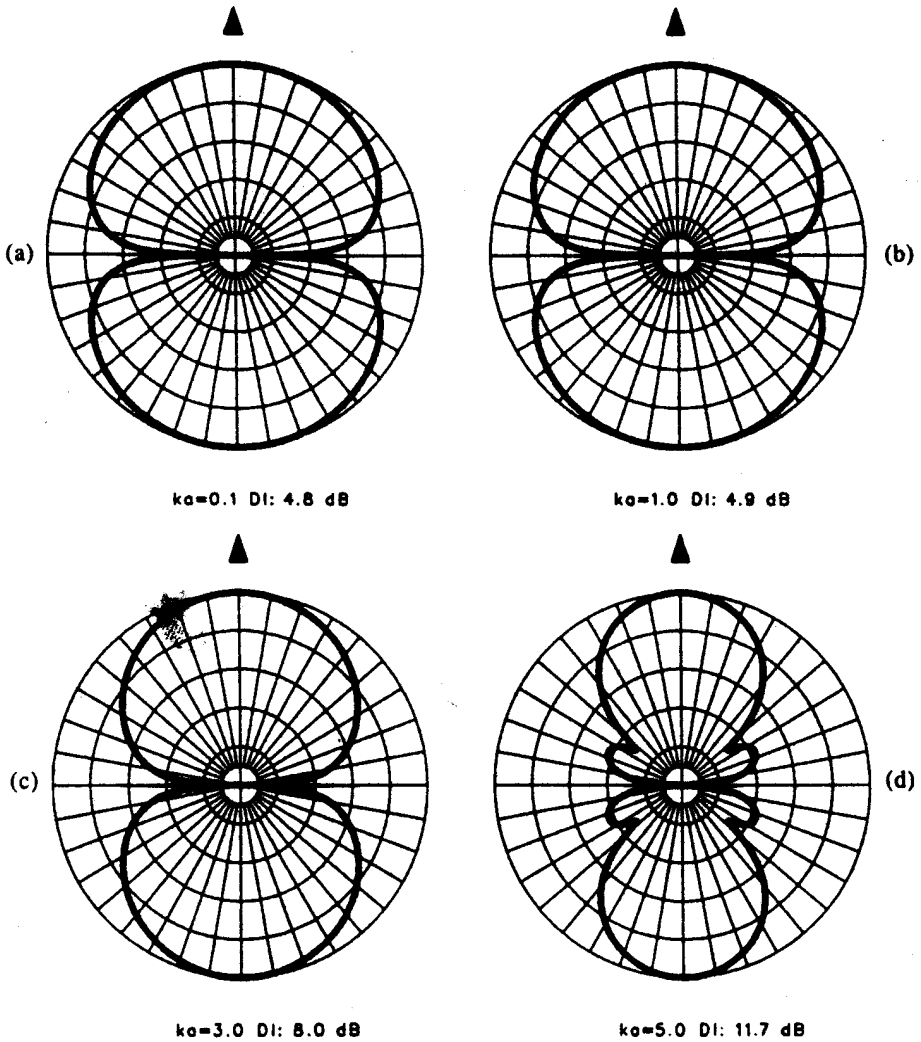

Fig. 10. Far-field polar patterns of vibrating membrane. The polar patterns are calculated for a membrane with parameters as in Fig. 2. Radial grid spacing 10 d/B, tangential grid spacing 10°. (a) $ka = 0.1$. (b) $ka = 1$. (c) $ka = 3$. (d) $ka = 5$.

of the slit impedance between the membrane and the electrodes. For this, formulas are given in [9]. It must be mentioned, however, that the influence of the slit as well as that of the perforations (provided the holes are large enough) are hardly noticed in this case. In Fig. 14 we see a comparison of the calculated and the

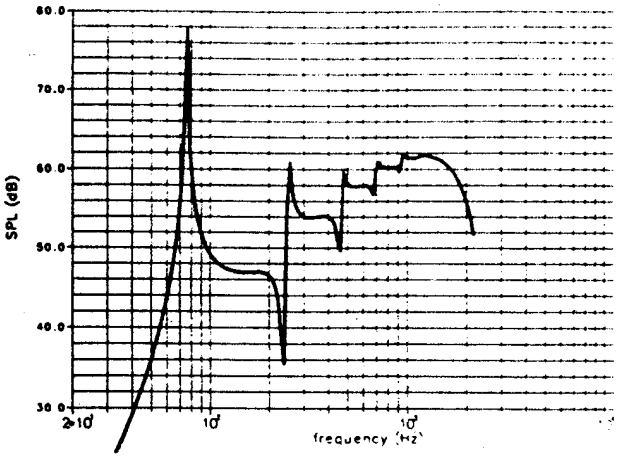

Fig. 11. Calculated SPL at 1 m, 45° off axis. The SPL response is calculated for a membrane with parameters as in Fig. 2.

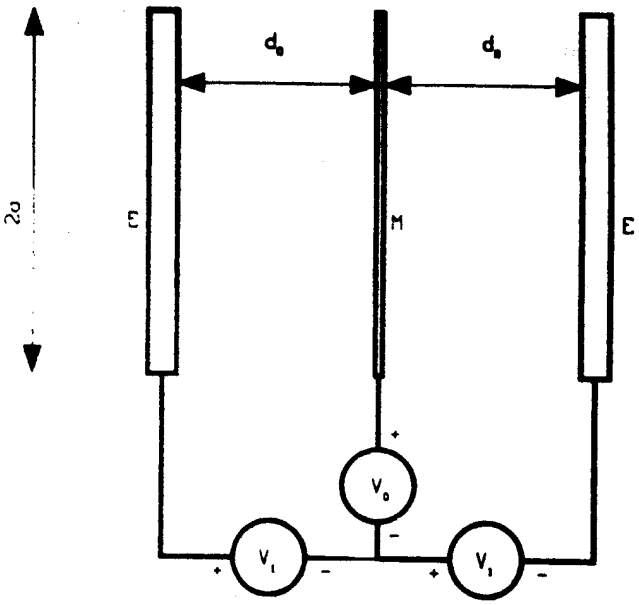

Fig. 13. Experimental setup of circular electrostatic loudspeaker. The membrane M is clamped along its circumference between two stationary electrodes E and charged by a dc source V_0. The electrostatic driving force is generated by means of two ac sources V_1, which drive the electrodes in opposite phase.

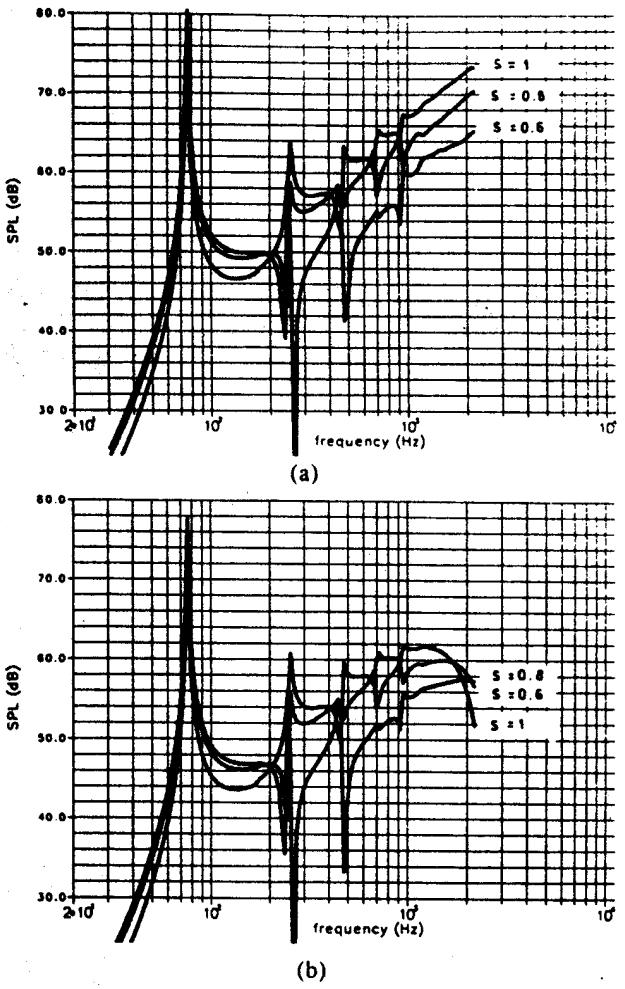

Fig. 12. Calculated SPL at 1 m. Calculations are carried out for reduced radiating area. The driving force is nonzero only for $0 \leq r \leq s$; other parameters as in Fig. 2. (a) On-axis response. (b) 45° off-axis response.

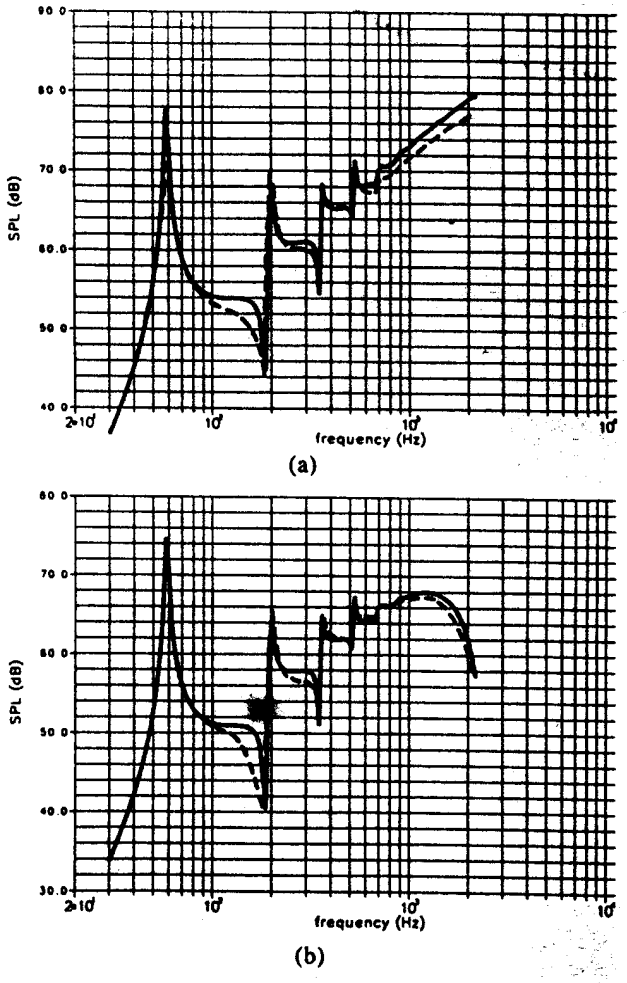

Fig. 14. Calculated and measured SPL of electrostatic loudspeaker. Response of a 250-mm-diameter electrostatic push–pull loudspeaker at 1 m. Solid lines—calculated; dashed lines—measured. Parameters are given in text. (a) On-axis response. (b) 45° off-axis response.

measured SPL at 1 m for this loudspeaker. Fig. 14(a) gives the on-axis response whereas Fig. 14(b) shows the 45° off-axis response. As can be seen, the agreement is quite good, which is a clear validation of the theoretical model.

4 CONCLUSIONS

In this paper we discussed the analysis of sound radiation from circular stretched membranes in air. It has been shown that the interaction of air and membrane is very important in the region around $ka = 1$ and that the rigid piston model is not capable of describing the vibrational behavior of the membrane. The proposed numerical procedure, derived from the exact theoretical model, may be used to predict the sound radiation from circular vibrating membranes, in this case electrostatic push–pull loudspeakers. The procedure may therefore be considered to be a useful tool in the analysis and computer-aided design of circular stretched-membrane transducers.

5 REFERENCES

[1] C. J. Bouwkamp, *Theoretische en numerieke behandeling van de buiging door een ronde opening* (Wolters, Groningen, 1941).

[2] A. Leitner, "Diffraction of Sound by a Circular Disk," *J. Acoust. Soc. Am.*, vol. 21, pp. 331–334 (1949).

[3] F. M. Wiener, "On the Relation between the Sound Fields Radiated and Diffracted by Plane Obstacles," *J. Acoust. Soc. Am.*, vol. 23, pp. 697–700 (1951).

[4] L. L. Beranek, *Acoustics* (McGraw-Hill, New York, 1954).

[5] P. J. Walker, "Wide Range Electrostatic Loudspeakers, Pt. 2, Problems of Air Loading," *Wireless World* (1955 June).

[6] J. H. Streng, "Calculation of the Surface Pressure on a Vibrating Circular Stretched Membrane in Free Space," *J. Acoust. Soc. Am.*, vol. 82, pp. 679–686 (1987).

[7] D. G. Crighton, "The Green Function of an Infinite, Fluid Loaded Membrane," *J. Sound Vibration*, vol. 86, pp. 411–433 (1983).

[8] F. V. Hunt, *Electroacoustics* (Wiley, New York, 1954).

[9] Z. Skvor, "On the Acoustical Resistance due to Viscous Losses in the Air Gap of Electrostatic Transducers," *Acustica*, vol. 19, pp. 296–299 (1967).

APPENDIX
NUMERICAL EVALUATION OF THE VIBRATING MEMBRANE

The surface pressure on a vibrating stretched membrane, the radiated sound field, and the membrane deflection may be calculated from the following procedure. The mathematical background is given in [6].

A.1 Input of External Parameters

On entry, the numerical values of the following parameters are given: air density ρ_0 [kg m^3], sound velocity c_0 [m s], membrane radius a [m], density ρ_m [kg/m^2], and tension T [N m], excitation frequency ω [rad/s], and amplitude of the time-harmonic driving force F [N m^{-2}]. There may be other external forces acting upon the membrane, such as additional acoustic damping. If these additional forces $F_a(r)$ [N m^{-2}] may be written as $F_a(r) = -j\omega\eta(r)z_s$, then the value of the (complex) impedance z_s must also be given.

A.2 Calculate Internal Parameters

From the input parameters we calculate three internal parameters α, β, and γ:

$$\alpha = a\left(\frac{\omega^2\rho_m - j\omega z_s}{T}\right)^{1/2}, \qquad \beta = ka,$$

$$\gamma = a\omega\left(\frac{2a\rho_0}{T}\right)^{1/2} \tag{22}$$

where α denotes the normalized membrane wave number, β the normalized wave number in air, and γ is a fluid-loading parameter.

A.3 Calculate Series Expansion Coefficients

The coefficients τ_n, $n = 1, \ldots, N$, are calculated from a set of linear equations,

$$\sum_{n=1}^{N} \tau_n\left[\sum_{m=1}^{M} \Psi_n(r_m)\Psi_i(r_m)\right] = \sum_{m=1}^{M} \Psi_i(r_m)\Phi(r_m),$$
$$i = 1, \ldots, N, \quad r_m = \frac{m}{M}a. \tag{23}$$

The functions $\Psi_n(r)$ are defined as

$$\Psi_n(r) = \sum_{k=1}^{K} \frac{2\gamma^2 J_0(j_{0k}r/a)J_{n+1/2}(j_{0k})}{J_1^2(j_{0k})(\alpha^2 - j_{0k}^2)j_{0k}^{n+1/2}}$$
$$+ j\left(\frac{1}{\beta}\right)^{n-1/2} \int_0^1 \left(\frac{1}{t}\right)^{n+1/2} (1 - t^2)^{1/2}$$
$$\times J_0\left(\frac{\beta t r}{a}\right)J_{n+1/2}(\beta t)\, dt$$
$$- \left(\frac{1}{\beta}\right)^{n-1/2} \int_0^{\pi/2} (2\sin\phi)^{1/2}\mathrm{Im}\left[e^{j[\phi(1-n)+\pi/2]}\right.$$
$$\left.\times J_0\left(\beta e^{j\phi}\frac{r}{a}\right)H_{n+1/2}^{(1)}(\beta e^{j\phi})\right] d\phi \tag{24}$$

where $J_0(x)$ and $J_{n+1/2}(x)$ are Bessel functions of the first kind, $H^{(1)}_{n+1/2}(x)$ is a Bessel function of the third kind (or Hankel function), and j_{0k} denotes the kth positive zero of the Bessel function $J_0(x)$. The values of K, M, and N are discussed below.

The function $\Phi(r)$ is calculated from

$$\Phi(r) = \sum_{k=1}^{K} \frac{2 J_0(j_{0k} r/a)}{J_1^2(j_{0k}) j_{0k}(\alpha^2 - j_{0k}^2)} \qquad (25)$$

Eq. 25 must be used in the case of a uniform driving force. The case of a nonuniform, steplike driving force must be evaluated by means of a different expression for $\Phi(r)$. Eq. (26) must be used when the membrane is driven at a section $0 \leq r \leq s$, $0 < s < a$, that is, when an inner part of the membrane is driven. When the outer part is driven, that is, the section $s \leq r \leq a$, $0 < s < a$, a combination of Eqs. (25) and (26) must be used.

$$\Phi(r) = \sum_{k=1}^{K} \frac{2(s/a)\, J_0(j_{0k} r/a) J_1(j_{0k} s/a)}{J_1^2(j_{0k}) j_{0k}(\alpha^2 - j_{0k}^2)} . \qquad (26)$$

The values of K, M, and N define the points where infinite summations are truncated. The choice is not trivial and depends on the situation in question. In this paper the results were obtained from $K = 320$, $M = 30$; the value of N varies from $N = 5$ ($ka \approx 0.1$) to $N = 10$ ($ka \approx 2$).

A.4 Calculate Surface Pressure and Membrane Excursion

Once the coefficients τ_n, $n = 1, \ldots, N$, are calculated, the surface pressure $p_+(r)$ on the membrane is given by

$$p_+(r) = \frac{a\omega^2 \rho_0 F}{T} \sum_{n=1}^{N} \frac{\tau_n (a^2 - r^2)^{n+1/2}}{2^{n+1/2} \Gamma(n + 3/2)} \qquad (27)$$

where $\Gamma(x)$ is the gamma function of argument x. The membrane excursion $\eta(r)$ may be calculated from

$$\eta(r) = \frac{a^2 F}{T} \left[-\Phi(r) + \sum_{n=1}^{N} \tau_n \sum_{k=1}^{K} \frac{2\gamma^2 J_0(j_{0k} r/a) J_{n+1/2}(j_{0k})}{J_1^2(j_{0k})(\alpha^2 - j_{0k}^2) j_{0k}^{n+1/2}} \right] \qquad (28)$$

where the function $\Phi(r)$ is defined in Eq. (25) or (26), depending on the situation, as explained in Appendix A.3.

A.5 Calculate the Sound Pressure Field

The sound pressure $p(r, z)$ at any point in space may be calculated from

$$p(r, z) = \frac{a^3 \omega^2 \rho_0 F}{T} \sum_{n=1}^{N} \tau_n \int_0^{\infty} \left(\frac{1}{\mu}\right)^{n+1/2} \times J_0\left(\frac{\mu r}{a}\right) J_{n+1/2}(\mu)\, e^{-j\sigma z/a}\, d\mu, \qquad z > 0 \qquad (29)$$

where

$$\sigma = \begin{cases} \sqrt{\beta^2 - \mu^2}, & \mu \leq \beta \\ -j\sqrt{\mu^2 - \beta^2}, & \mu > \beta \end{cases}$$

$$p(r, z) = -p(r, -z) \qquad z < 0$$

$$p(r, 0) = 0, \qquad r > a$$

$$p(r, 0^+) = p_+(r), \qquad r \leq a$$

$$p(r, 0^-) = -p(r, 0^+), \qquad r \leq a .$$

THE AUTHOR

Johannes Hermannus (Hans) Streng was born in Apeldoorn, The Netherlands, in 1954. He received a degree in automotive engineering from Apeldoorn Polytechnic in 1976. He then studied electrotechnical engineering at the Eindhoven University of Technology, where he earned a degree in 1984. His thesis was on calculation of relectorantenna radiation.

At the present time he is in an MBA program of the University of Rochester, New York, and the Erasmus University of Rotterdam, The Netherlands. He is employed at Philips Research Laboratories, Eindhoven, in the Department of Acoustics and Noise Control, where he is researching sound radiation for transducer applications.